

UNIR-Net: A Novel Approach for Restoring Underwater Images with Non-Uniform Illumination Using Synthetic Data

Ezequiel Perez-Zarate^a, Chunxiao Liu^a, Oscar Ramos-Soto^b, Diego Oliva^{b,*}, Marco Perez-Cisneros^b

^a*School of Computer Science and Technology, Zhejiang Gongshang University, Hangzhou, 310018, Zhejiang, China*

^b*Departamento de Ingeniería Electro-fotónica, Universidad de Guadalajara, CUCEI, Av. Revolución 1500, Guadalajara, 44430, Jal., México*

Abstract

Enhancing underwater images with non-uniform illumination (NUI) is crucial for improving visibility and visual quality in marine environments, where image degradation is caused by significant absorption and scattering effects. However, traditional model-based methods are often ineffective at capturing the complex illumination variations present in such images, resulting in limited visual improvements. On the other hand, learning-based approaches have shown promising results but face challenges due to the lack of specific datasets designed to effectively address the non-uniform illumination problem. To overcome these challenges, the Underwater Non-uniform Illumination Restoration Network (UNIR-Net) is introduced, a novel method that integrates illumination enhancement and attention blocks, along with visual refinement and contrast correction modules. This approach is specifically designed to mitigate the scattering and absorption effects that cause light attenuation in underwater environments. Additionally, the Paired Underwater Non-uniform Illumination (PUNI) dataset is presented, a paired resource that facilitates the restoration of underwater images under non-uniform illumination conditions. Extensive experiments conducted on the PUNI dataset and the large-scale real-world Non-Uniform Illumination Dataset (NUID), which contains underwater images with non-uniform illumination, demonstrate the robust generalization ability of UNIR-Net. This method outperforms existing approaches in both quantitative metrics and qualitative evaluations. Furthermore, UNIR-Net not only significantly enhances the visual quality of images but also improves performance in advanced computer vision tasks, such as semantic segmentation in underwater environments, highlighting its broad applicability and potential impact. The code of this method is available at <https://github.com/xingyumex/UNIR-Net>

Keywords: Non-uniform illumination, Light attenuation, Underwater imaging, Low-level vision, Deep learning

1. Introduction

Underwater images are captured under non-uniform illumination conditions which present significant challenges due to the absorption and scattering of light in submarine environments. This phenomenon leads to loss of detail, low visibility, and a marked degradation of contrast, affecting visual quality and hindering accurate interpretation of the images [1]. As depth increases, natural light diminishes drastically, making the use of artificial illumination essential. However, these light sources often produce uneven illumination, concentrating light in specific areas of the image. This results in overexposed zones at the center and underexposed regions at the periphery, causing the loss of critical details and complicating information recovery for detailed analysis.

Model-based and Learning-Based methods have been developed to enhance underwater images; however, most of them focus on general problems, such as contrast enhancement [2], color correction [3], underwater haze removal, or blur reduction [4]. Nonetheless, few studies have specifically addressed the unique challenges associated with

*Corresponding author

Email addresses: isaias.perez@alumnos.udg.mx (Ezequiel Perez-Zarate), cxliu@zjgsu.edu.cn (Chunxiao Liu), oscar.ramos9279@alumnos.udg.mx (Oscar Ramos-Soto), diego.oliva@cucei.udg.mx (Diego Oliva), marco.perez@cucei.udg.mx (Marco Perez-Cisneros)

non-uniform illumination in underwater environments. Recent methods [5, 6, 7, 8] have started to focus on this issue, aiming to simultaneously correct overexposed and underexposed regions without introducing additional distortions.

Building upon these efforts, advancements in applications such as Autonomous Underwater Vehicles (AUVs) [9, 10] and Remotely Operated Vehicles (ROVs) [11] have been instrumental in the development of new methods to address non-uniform illumination in underwater images. These innovations are crucial not only to overcome challenges in ocean exploration but also to enhance precision in tasks such as object detection[12] and semantic segmentation[13] in underwater environments.

1.1. Motivation

The correction of non-uniform illumination in underwater images represents a key challenge in improving their visual quality and optimizing their utility in various practical applications. Although progress has been made with model-based and deep learning methods, significant limitations persist, such as loss of fine details and lack of generalization capability. Methods designed to enhance low-light images in terrestrial environments [14, 15, 16, 17, 18, 19, 20] are unsuitable for underwater settings, as they often produce a haze effect across the entire image. This is due to the unique properties of the aquatic medium, which include light scattering and selective absorption of colors, particularly at wavelengths corresponding to red [21]. As a result, images processed by these methods tend to acquire a characteristic greenish tone, reflecting the inability of these algorithms to adequately address the optical properties of water.

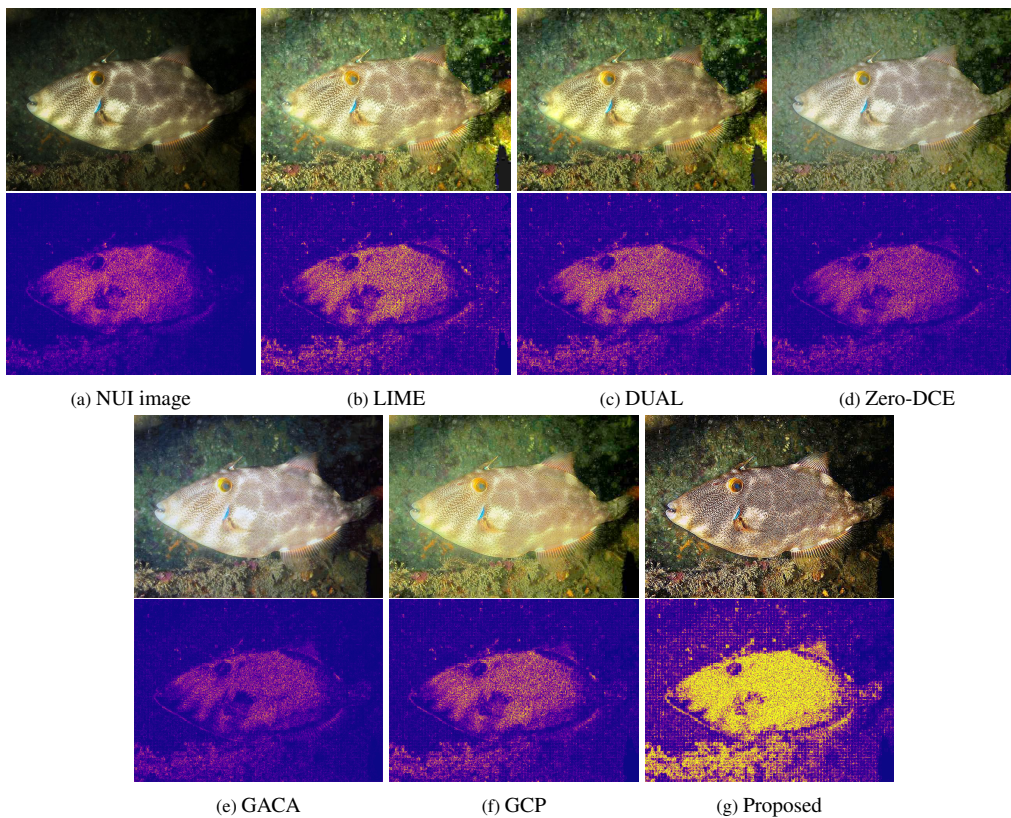


Figure 1: Comparison of in-air enhancement methods and the proposed method.

Figure 1 presents a comparison between in-air low-light enhancement methods and the proposed method, applied to underwater images with non-uniform illumination, along with their contrast maps. Most of these methods produce results with greenish tones and haze effects, highlighting their limitations. In contrast, the method proposed in this work demonstrates superior performance by preserving structural details and improving visual quality in scenarios with non-uniform illumination.

Given the importance of underwater images in fields such as underwater archaeology, ocean exploration, and environmental monitoring, it is essential to develop algorithms specifically tailored to address the complexities associated with non-uniform illumination. This involves not only correcting exposure and contrast but also preserving key details, accurately correcting chromatic deviations, and enhancing critical edges and textures.

1.2. Contributions

This paper introduces the Underwater Non-uniform Illumination Restoration Network (UNIR-Net) to overcome the challenge of enhancing underwater images captured under non-uniform illumination conditions, a recurring problem in real-world underwater applications. The main contributions of this research are as follows:

- **A novel approach for enhancing underwater images with non-uniform illumination:** UNIR-Net is proposed as a method specifically designed to restore images affected by uneven illumination. This model integrates specialized blocks for illumination enhancement, attention mechanisms, and modules for visual refinement and contrast correction.
- **A novel synthetic paired dataset:** The Paired Underwater Non-uniform Illumination (PUNI) is introduced as a dataset designed to address the lack of paired datasets exclusively representing underwater images with non-uniform illumination.
- **Validation in practical underwater applications:** The proposed approach is validated by applying it as a preprocessing method for semantic segmentation tasks, demonstrating its effectiveness in real-world underwater scenarios.

2. Related Work

In this section, the most relevant previous approaches in underwater image enhancement are presented, focusing on model-based methods and learning-based methods, highlighting their strengths, limitations, and key contributions.

2.1. Model-Based Methods

Model-based methods rely on mathematical and physical models to enhance images, leveraging established theories about light behavior. Unlike data-driven approaches, these methods operate independently of large datasets, focusing instead on the intrinsic properties of illumination and image formation.

In 2016, Guo et al. [14] proposed a low-light image enhancement method (LIME) that estimates the illumination of each pixel by using the maximum value of the R, G, and B channels. The illumination map is subsequently refined by applying a structural prior. Three years later, in 2019, Zhang et al. [15] presented an automatic exposure correction method that uses a dual estimation of illumination to correct underexposed and overexposed regions. The corrected images are then fused using a multiple-exposure fusion technique to obtain a globally well-exposed image. Later in 2020, Marques and Albu introduced L²UWE [5], an underwater low-light image enhancer that uses contrast models to estimate illumination. Two enhanced images are fused, emphasizing luminance and local contrast. In the same year, Yuan et al. [22] proposed an underwater image enhancement method using Contour Bougie (CB) morphology. It enhances scene contours and visibility through morphological operations with two structuring elements. The images are then normalized and stretched to improve white balance in the RGB channels.

Moving to 2021, Xie et al. [23] proposed a variational framework guided by the red channel to enhance underwater images affected by low contrast, fog, and blur, incorporating forward scattering and blur kernel estimation in the refinement process. In 2022, Zhang et al. [2] presented a method for enhancing underwater images by correcting colors, improving contrast, and sharpening details using attenuation matrices, histogram-based techniques, and a multi-scale unsharp mask. In the same year, Zhuang et al. [24] introduced a Retinex variational model with hyper-laplacian reflectance priors for underwater image enhancement. It uses $l_{1/2}$ and l_2 norms to enhance fine details and structures while estimating illumination. Similarly, Zhang et al. [25] proposed MLLE, an underwater image enhancement method that adjusts color, details, contrast, and balances color in the CIELAB space, producing vivid colors and improved contrast.

More recently, in 2023, Hou et al. [7] proposed a variational framework with an Illumination Channel Sparsity Prior (ICSP) to restore underwater images, enhancing brightness, correcting color distortions, and highlighting details using a Retinex-based model with L_0 norm constraints. In the same year, Zhang et al. [26] introduced a method for underwater image enhancement using piecewise color correction and dual prior-based contrast enhancement, applying gain-based color correction and decomposing the base and detail layers in the V channel of HSV. Another contribution by Zhang et al. [27] presented a technique called WWPF for underwater image enhancement, which corrects color distortion using an attenuation map, improves both global and local contrast, and fuses the images through a wavelet visual perception strategy to produce high-quality results.

Finally, in 2024, An et al. [28] proposed a hybrid fusion method (HFM) to enhance underwater images, addressing issues such as white balance distortion, color shift, low visibility, and contrast. The method incorporates color correction, visibility recovery, and contrast enhancement through fusion techniques. Additionally, Jeon et al. [18] presented a fast low-light image enhancement method based on an atmospheric scattering model. The transmission map is calculated using the average and maximum values of the original image, which are estimated with gamma correction.

Model-based methods offer the advantage of not relying on extensive datasets and provide interpretable results grounded in theory. However, struggling with generalization to diverse scenarios is common, as reliance on predefined assumptions can limit performance compared to data-driven approaches, especially in complex or highly variable image degradation conditions.

2.2. Learning-Based Methods

Learning-based methods have gained significant attention in low-level vision tasks due to their ability to learn complex patterns from large datasets. By leveraging deep/machine learning models, these methods effectively address various image distortions and enhance visual quality across a wide range of tasks. Their capacity to learn from diverse data allows them to generalize well, providing efficient and scalable solutions for real-world image enhancement challenges.

In 2020, Guo et al. [16] introduced Zero-DCE, a method for light enhancement using image-specific curve estimation with a lightweight deep network. It adjusts dynamic range without requiring paired data, using non-reference loss functions for efficient image enhancement across diverse lighting conditions. In 2021, Naik et al. [29] propose UWnet, a lightweight neural network architecture for underwater image enhancement, designed to balance effectiveness with reduced computational complexity. The next year, in 2022, Xie et al. [30] propose a deep learning-based underwater image enhancement network tailored for low-light environments, addressing both low-light degradation and scattering effects. Later in 2023, Wen et al. [31] proposed SyreaNet, a framework for underwater image enhancement that combines synthetic and real data. It uses a revised image formation model and domain adaptation strategies, along with an image synthesis module and a disentangled network, to predict clearer images. In the same year, Li et al. [3] introduced a template-free color transfer learning framework for underwater image enhancement, predicting transfer parameters with attention-driven modules for more flexible and robust enhancement. Similarly, Shen et al. [4] proposed UDAformer, a dual attention transformer for underwater image enhancement. It combines channel and pixel self-attention transformers, uses a shifted window technique for efficiency, and restores images with residual connections.

More recently, in 2024, Yao et al. [17] proposed the Gradient-Aware and Contrastive-Adaptive (GACA) framework for low-light image enhancement, using accurate gradient estimation as a structural prior and a novel regularization constraint to address color abnormalities and artifacts. In the same year, Zhang et al. [32] introduced LENet, a lightweight underwater image enhancement network using depthwise separable convolution, one-shot aggregation, and a squeeze-and-excitation module to reduce complexity and improve feature extraction. In addition, Zhang et al. [33] proposed SMDR-IS, a method for enhancing underwater details using multi-scale refinement. It employs the Adaptive Selective Intrinsic Supervised Feature (ASISF) module for detail propagation and the Bifocal Intrinsic-Context Attention (BICA) module in the encoder-decoder framework to improve spatial context and restoration. Finally, Park and Eom [34] proposed a method with an adaptive standardization network to correct distortion and a normalization network using squeeze-and-excitation blocks to enhance contrast, remove haze, and restore brightness.

By leveraging large datasets to learn diverse patterns, these methods effectively address complex distortions in low-level vision tasks. While requiring extensive labeled data and computational resources, their ability to generalize makes them highly effective across a wide range of image enhancement challenges.

3. Materials and Methods

3.1. Underwater Image Generation Dataset

In this section, the Paired Underwater Non-uniform Illumination (PUNI) dataset is introduced for training and evaluating techniques aimed at improving underwater images with non-uniform illumination. The process of acquiring and selecting the underwater images is described in detail. Subsequently, the synthesis process of the images is discussed to produce scenarios with non-uniform illumination in underwater environments. The complete data generation diagram is shown in Fig. 2.

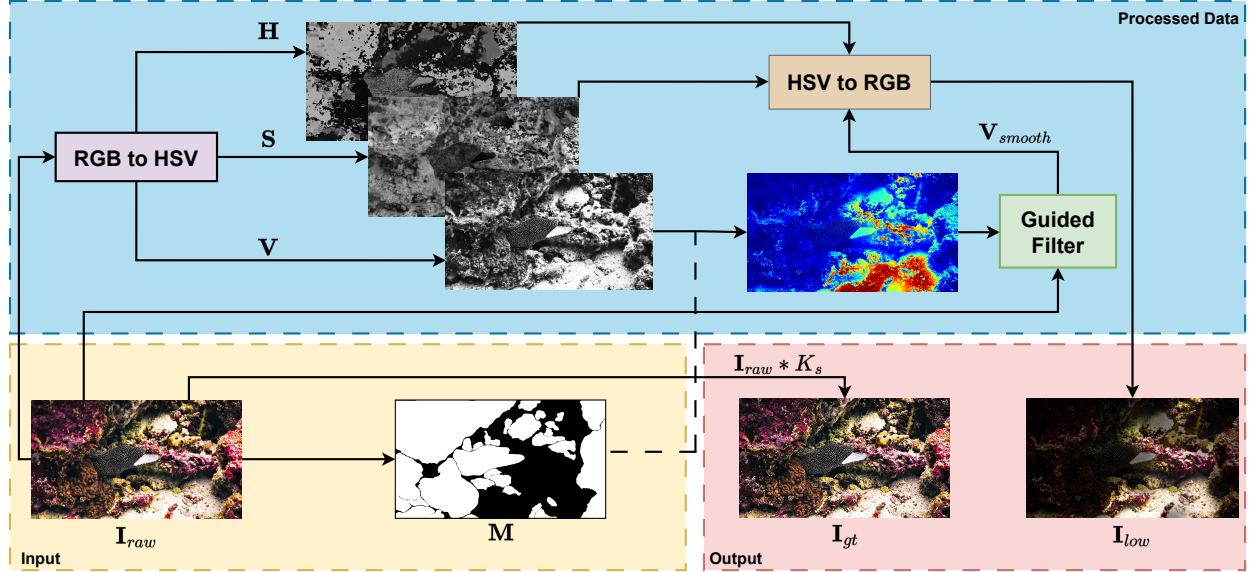


Figure 2: Diagram for the PUNI dataset generation.

3.1.1. Underwater Image Selection

The enhancement of underwater images has been extensively studied through benchmarks like Enhanced Underwater Visual Perception (EUVP) [35], Underwater Image Enhancement Benchmark (UIEB) [36], and Low-light Underwater Image Enhancement (LUIE) [30], which aim to address challenges related to contrast, color fidelity, and illumination in low-light scenarios. Despite their contributions, these approaches face notable drawbacks in terms of preserving resolution and generating high-quality outputs. The raw images provided by existing datasets frequently exhibit inherent flaws, including insufficient detail, color distortions, blurring artifacts, and uneven lighting. Additionally, the presence of fog-like effects often obscures essential visual information. Such limitations not only hinder the datasets' utility for producing synthetic data with non-uniform illumination but may also introduce undesirable biases in training pipelines, ultimately compromising the performance and generalization of enhancement models.

Figure 3 shows representative examples from these datasets. For instance, Fig.3a, taken from the EUVP dataset, reveals that most pixel intensities in its RGB histogram are concentrated in the center, resulting in a predominant fog effect in the image. In the case of Fig. 3b, corresponding to the UIEB dataset, most pixel intensities shift towards the left side in the red channel, while in the green and blue channels, they concentrate in the center. Additionally, this image exhibits low-quality textures with noticeable noise in certain areas. Lastly, the image from the LUIE dataset shown in Fig. 3c displays a motion effect that affects its clarity. In its RGB histogram, pixel intensities are primarily distributed in the center, reflecting visual quality issues. In contrast, most of the images collected for creating the Paired Underwater Non-uniform Illumination (PUNI) dataset present a more uniform distribution of pixel intensities in the histogram. This results in better visual quality in terms of texture and lighting, as shown in Fig. 3d.

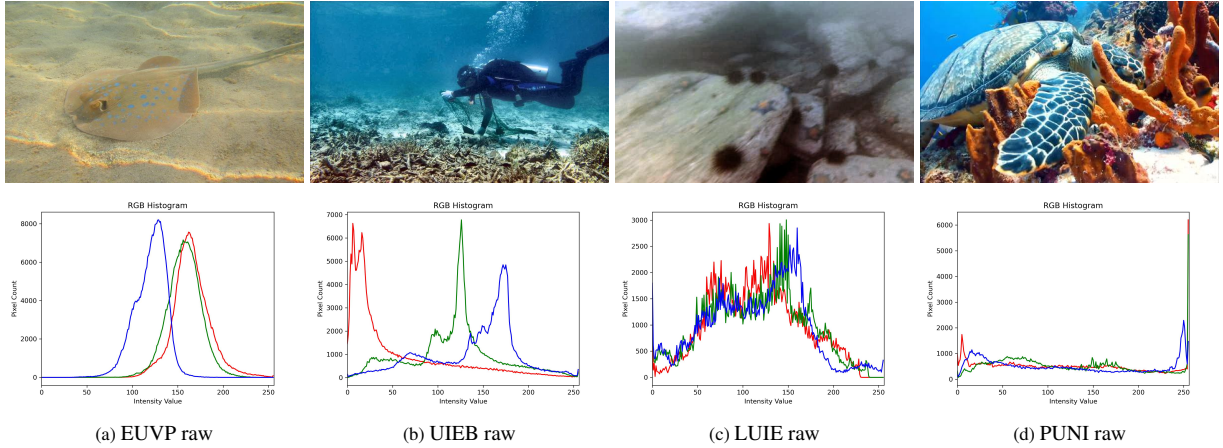


Figure 3: Comparative analysis of various underwater datasets in raw images.

The limitations present in most raw images from the EUVP, UIEB, and LUIE underwater datasets underscore the need to develop a new, higher-quality raw dataset that can better synthesize the challenges associated with non-uniform illumination in underwater environments. For this purpose, 3,277 high-resolution, copyright-free images were carefully collected from a human perspective using platforms like Unsplash and Freepik. These images were selected following strict criteria such as color accuracy, absence of blur, proper lighting, and no fog. This set of high-quality images serves as the foundation for the design of the new PUNI dataset.

3.1.2. Synthesis with Non-Uniform Illumination

Non-uniform illumination in underwater environments is a distinctive feature caused by the absorption and scattering of light in water, which prevents it from propagating evenly. In this context, paired terrestrial datasets commonly used for low-light image enhancement [37, 38, 39] are ineffective, as they fail to account for the absorption and scattering phenomena inherent to aquatic environments. Consequently, training models with these datasets leads to undesired effects in the images, such as haze and inaccurate color tones.

Synthesizing a dataset of low-light images with non-uniform illumination has been previously explored to train models for enhancing terrestrial images under poor lighting conditions [40]. However, this approach proves inadequate for underwater images due to the inherent differences between terrestrial and aquatic environments. A notable aspect of the synthesis method in [40] is the application of superpixel-based segmentation [41] to divide images into regions and simulate illumination variations within these segments.

In contrast, this work adopts the Segment Anything Model (SAM) [42], an advanced method capable of automatically identifying and segmenting objects in images. SAM enables the generation of binary masks from pre-collected raw underwater images, as depicted in Fig. 3d, to construct an initial underwater dataset. These binary masks allow selective attenuation of specific image areas, effectively replicating the non-uniform illumination conditions characteristic of underwater environments. The complete synthesis process for generating underwater images with non-uniform illumination is outlined in **Algorithm 1**.

The process starts with an input image represented as $\mathbf{I}_{raw} \in \mathbb{R}^{H \times W \times 3}$, where H and W are the dimensions of the RGB image. A binary mask $\mathbf{M} \in \{0, 1\}^{H \times W}$ is generated using SAM, where masked pixels are assigned a value of 1. Subsequently, the raw RGB image \mathbf{I}_{raw} is converted into the HSV color space, resulting in $\mathbf{I}_{HSV} \in \mathbb{R}^{H \times W \times 3}$. From this, the V channel, denoted as $\mathbf{V} \in \mathbb{R}^{H \times W}$, is extracted. The masked region in the V channel, \mathbf{V}_{masked} , is defined as follows:

$$\mathbf{V}_{masked} = \{\mathbf{V}_{i,j} \mid \mathbf{M}_{i,j} > 0\} \quad (1)$$

where $\mathbf{V}_{masked} \in \mathbb{R}^{H \times W}$ represents the masked area in the V channel, $\mathbf{V}_{i,j}$ is the pixel value at position (i, j) , and $\mathbf{M}_{i,j}$ is the corresponding mask value. The average brightness of the masked values, $\mathbf{B}_{average}$, is computed as:

Algorithm 1 Underwater Image Synthesis with Non-Uniform Illumination

Require: RGB image raw \mathbf{I}_{raw} ; Binary mask \mathbf{M} ; Brightness threshold α , Guided Filter Kernel K_g

Ensure: Synthetic non-uniform illumination image \mathbf{I}_{low}

- 1: Convert $\mathbf{I}_{raw} \rightarrow \mathbf{I}_{HSV}$
 - 2: Extract \mathbf{V} channel from \mathbf{I}_{HSV}
 - 3: Average brightness $\mathbf{B}_{average}$ of the masked area \mathbf{V}_{masked}
 - 4: **if** $\mathbf{B}_{average} < \alpha$ **then**
 - 5: Apply "Deepen" adjustment to the masked area \mathbf{V}_{masked}
 - 6: $\mathbf{V}^\lambda \leftarrow Adjust\ Brightness(\mathbf{V}, "Deepen")$
 - 7: **else**
 - 8: Randomly choice apply "Surface", "Deepen", or "None" adjustment to the masked area \mathbf{V}_{masked}
 - 9: $\mathbf{V}^\lambda \leftarrow Adjust\ Brightness(\mathbf{V}, "Random\ Choice")$
 - 10: **end if**
 - 11: Compute $\mathbf{V}_{smooth} \leftarrow Guided\ Filter(\mathbf{I}_{raw}, \mathbf{V}^\lambda, K_g)$
 - 12: Update $\mathbf{I}_{HSV} \leftarrow (\mathbf{H}, \mathbf{S}, \mathbf{V}_{smooth})$
 - 13: Convert $\mathbf{I}_{HSV} \rightarrow \mathbf{I}_{low}$
 - 14: **return** \mathbf{I}_{low}
-

$$\mathbf{B}_{average} = \frac{1}{|\mathbf{V}_{masked}|} \sum_{(i,j) \in \mathbf{V}_{masked}} \mathbf{V}_{i,j} \quad (2)$$

To determine the type of brightness adjustment for the segmented masks, a comparison between $\mathbf{B}_{average}$ and the predefined brightness threshold α , which is set to 70, is performed. This decision process is defined as:

$$\delta = \begin{cases} Deepen, & \text{if } \mathbf{B}_{average} < \alpha, \\ \text{Random}(\{Surface, Deepen, None\}), & \text{otherwise.} \end{cases} \quad (3)$$

where "Deepen" simulates low-light conditions typical of deeper and less illuminated areas, "Surface" simulates brighter conditions near the surface, and "None" implies no modification. The local brightness adjustment for the masked \mathbf{V} channel, \mathbf{V}^λ , depending on the selected operation δ , is expressed as follows:

$$\mathbf{V}^\lambda = \begin{cases} \beta \cdot \mathbf{V}^{\gamma_d}, & \text{if } \delta = \text{Deepen}, \\ \mathbf{V}^{\gamma_s}, & \text{if } \delta = \text{Surface}, \\ \mathbf{V}, & \text{otherwise.} \end{cases} \quad (4)$$

where, γ_d and γ_s are constant gamma correction values, β is a linear adjustment factor, and $\mathbf{V}^\lambda \in \mathbb{R}^{H \times W}$ represents the brightness-modified \mathbf{V} channel. The constant values are adopted from the synthesis parameters proposed in [40]. After adjusting the brightness in the segmented regions, a guided filter [43] is applied to produce more realistic textures under non-uniform illumination conditions. This process is defined as:

$$\mathbf{V}_{smooth} = \text{Guided Filter}(\mathbf{I}_{raw}, \mathbf{V}^\lambda, K_g) \quad (5)$$

where $\mathbf{V}_{smooth} \in \mathbb{R}^{H \times W}$ is the filtered image, and K_g is the kernel size of the filter. A kernel of 64×64 was chosen as it produced the best results, as shown in Fig. 4. Smaller kernels prominently highlight the mask boundaries, while larger kernels overly blur the image, diminishing the non-uniform illumination effect. Finally, \mathbf{V}_{smooth} replaces \mathbf{V} as follows:

$$\mathbf{I}_{HSV} = (\mathbf{H}, \mathbf{S}, \mathbf{V}_{smooth}) \quad (6)$$

The modified \mathbf{I}_{HSV} is then converted back to the RGB color space, resulting in the synthesized non-uniformly illuminated image \mathbf{I}_{low} . Once the non-uniformly illuminated input image \mathbf{I}_{low} is generated, the ground truth image \mathbf{I}_{gt} is created by applying a sharpening filter to enhance edges. Let K_s be the sharpening kernel defined as:

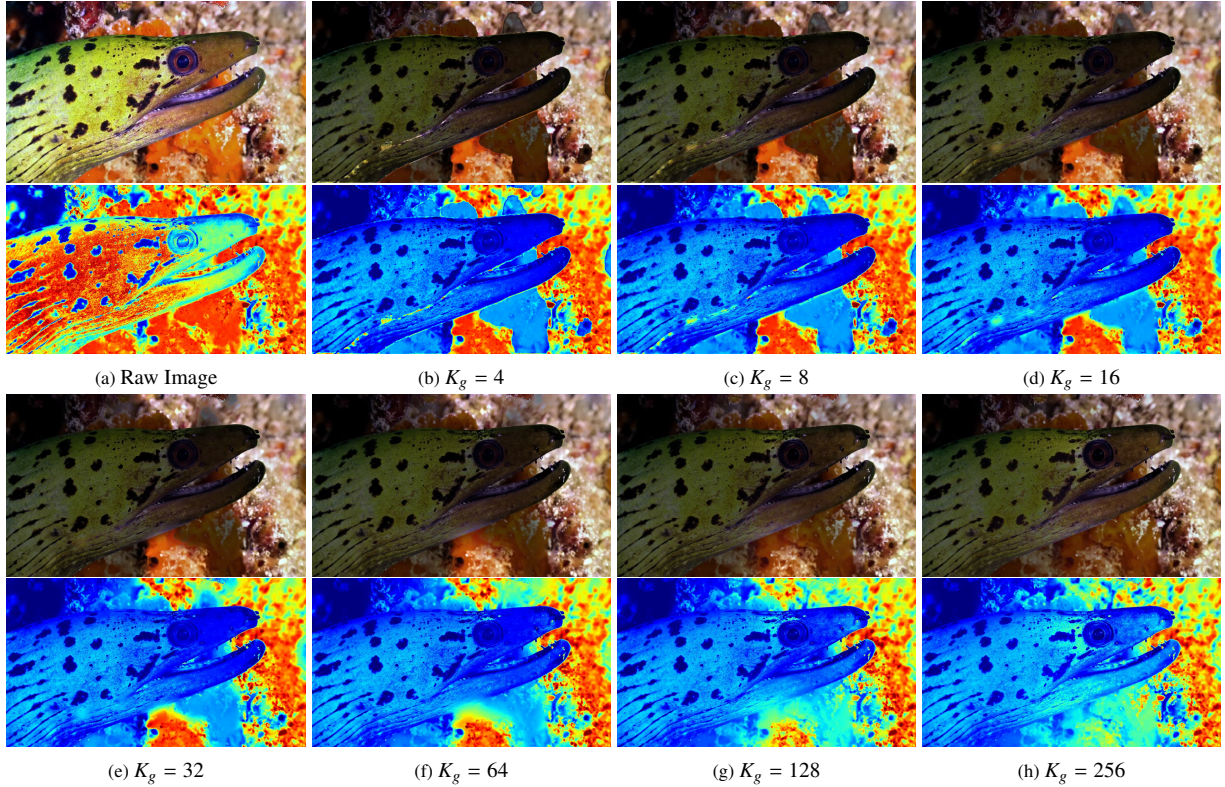


Figure 4: Visual comparison of results with different kernel sizes in the guided filter.

$$K_s = \begin{bmatrix} 0 & -1 & 0 \\ -1 & 5 & -1 \\ 0 & -1 & 0 \end{bmatrix} \quad (7)$$

To compute \mathbf{I}_{gt} , a channel-wise convolution is performed between the raw input image, \mathbf{I}_{raw} , and the kernel K_s . This operation is expressed as:

$$\mathbf{I}_{gt} = \mathbf{I}_{raw} * K_s \quad (8)$$

where, $*$ represents the convolution operator. The sharpened image \mathbf{I}_{gt} serves as the ground truth, providing an enhanced representation of edge information. This procedure finalizes the construction of the PUNI dataset, ensuring that it captures both non-uniform illumination and detailed edge features critical for training enhancement models.

3.2. UNIR-Net Design

This section presents the main study of this article, which consists of the development of the Underwater Non-Uniform Illumination Restoration Network (UNIR-Net) architecture. The primary objective of this network is to improve the visual perception of images captured in marine environments with non-uniform illumination. The design of UNIR-Net is structured around four essential components that ensure its optimal performance. The first component is the Illumination Enhancement Block (IEB), presented in Section 3.2.1. The second is the Attention Block (AB), described in Section 3.2.2. The third is the Visual Refinement Module (VRM), detailed in Section 3.2.3. Finally, the fourth component is the Contrast Correction Module (CCM), explained in Section 3.2.4. Fig. 5 shows the complete architecture, where the encoder part includes two IEBs, interspersed with an AB. The middle section combines one AB and one IEB, while the decoder includes an IEB and a convolution with a 3×3 kernel. Finally, the VRM and CCM modules are placed at the end of the process. This structure allows the architecture to effectively address local

and global variations in the illumination of the input image $\mathbf{I}_{low} \in \mathbb{R}^{H \times W \times 3}$, achieving a significant improvement in the lighting and visual perception of the resulting image $\mathbf{I}_{enh} \in \mathbb{R}^{H \times W \times 3}$

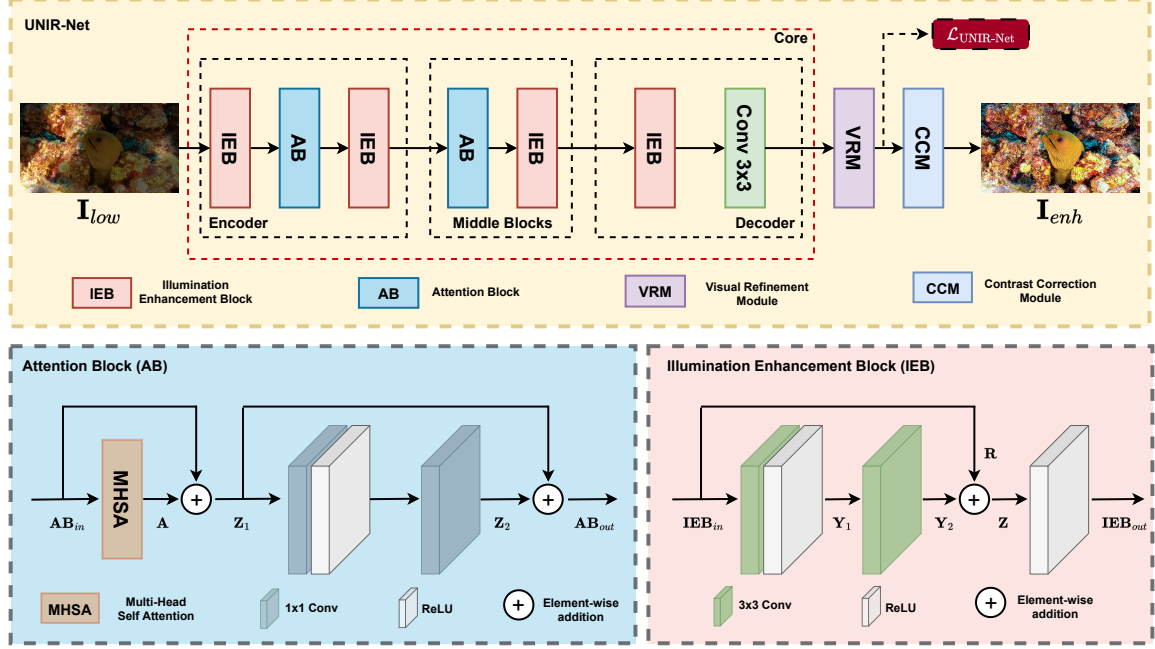


Figure 5: The architecture of UNIR-Net.

3.2.1. Illumination Enhancement Block (IEB)

The IEB is based on the use of convolutions, ReLU activation functions, and residual connections to enhance lighting features in underwater images. It operates on an input tensor $\mathbf{IEB}_{in} \in \mathbb{R}^{H \times W \times C_{in}}$, where C_{in} denotes the number of input channels, and H and W correspond to the spatial dimensions of the image. The enhancement process begins with a convolution operation performed using a filter \mathbf{W}_1 , which extracts key features from the input. This is immediately followed by the application of the ReLU activation function to introduce non-linearity, resulting in:

$$\mathbf{Y}_1 = \text{ReLU}(\mathbf{IEB}_{in} * \mathbf{W}_1) \quad (9)$$

Next, the intermediate features \mathbf{Y}_1 are refined through a second convolution with a filter \mathbf{W}_2 , resulting in:

$$\mathbf{Y}_2 = \mathbf{Y}_1 * \mathbf{W}_2 \quad (10)$$

If the number of input and output channels does not match ($C_{in} \neq C_{out}$), an adjustment filter \mathbf{W}_m is used. The residual \mathbf{R} is then computed as follows:

$$\mathbf{R} = \begin{cases} \mathbf{IEB}_{in} * \mathbf{W}_m, & \text{if } C_{in} \neq C_{out}, \\ \mathbf{IEB}_{in}, & \text{otherwise.} \end{cases} \quad (11)$$

Subsequently, the refined output \mathbf{Y}_2 is combined with the adjusted residual \mathbf{R} through an addition operation:

$$\mathbf{Z} = \mathbf{Y}_2 + \mathbf{R} \quad (12)$$

Finally, \mathbf{Z} passes through an additional ReLU activation to produce the final output of the block:

$$\mathbf{IEB}_{out} = \text{ReLU}(\mathbf{Z}), \quad (13)$$

where $\mathbf{IEB}_{out} \in \mathbb{R}^{H \times W \times C_{out}}$ contains the enhanced features. This output integrates both the original input information and the transformations performed by the convolutions, optimizing the lighting representation for subsequent stages of the model.

3.2.2. Attention Block

The Attention Block (AB) leverages a Multi-Head Self-Attention (MHSA) mechanism combined with a Feed-Forward Network (FFN) to effectively capture both spatial and contextual relationships within the features processed by a convolutional backbone. This design integrates two key components an MHSA module and an FFN enhanced by residual connections to retain the original feature representations from the input.

The process begins with an input tensor $\mathbf{AB}_{in} \in \mathbb{R}^{H \times W \times C}$, where H and W denote the spatial dimensions, and C represents the number of channels. The MHSA module extracts the query (\mathbf{Q}), key (\mathbf{K}), and value (\mathbf{V}) matrices using learned weight matrices through convolution operations, as expressed below:

$$\mathbf{Q} = \mathbf{W}_Q * \mathbf{AB}_{in}, \quad \mathbf{K} = \mathbf{W}_K * \mathbf{AB}_{in}, \quad \mathbf{V} = \mathbf{W}_V * \mathbf{AB}_{in} \quad (14)$$

where \mathbf{W}_Q , \mathbf{W}_K , and \mathbf{W}_V are trainable weight matrices, and $*$ indicates convolution. The attention mechanism is then formulated as:

$$\mathbf{A} = \text{softmax} \left(\frac{\mathbf{Q} \cdot \mathbf{K}^T}{\sqrt{\frac{C}{N_h}}} \right) \cdot \mathbf{V} \quad (15)$$

where N_h is the number of attention heads. This mechanism generates an attention-enhanced feature map \mathbf{A} , which is combined with the original input through a residual connection:

$$\mathbf{Z}_1 = \mathbf{A} + \mathbf{AB}_{in} \quad (16)$$

Subsequently, the FFN further processes \mathbf{Z}_1 to refine and enhance the extracted features. The FFN operation is defined as:

$$\mathbf{Z}_2 = \mathbf{W}_b * \text{ReLU}(\mathbf{W}_a * \mathbf{Z}_1) \quad (17)$$

where \mathbf{W}_a and \mathbf{W}_b are learnable matrices used to project features into higher-dimensional spaces and then reduce them back, respectively. Finally, the output of the FFN is combined residually with \mathbf{Z}_1 , yielding the final output of the AB:

$$\mathbf{AB}_{out} = \mathbf{Z}_1 + \mathbf{Z}_2 \quad (18)$$

This design ensures that the AB block not only captures intricate spatial and contextual relationships but also preserves critical information from the input features.

3.2.3. Visual Refinement Module

The Visual Refinement Module (VRM) is designed to refine image features within a defined range of 0 to 1, preventing pixel overflow and enhancing the visual clarity of the processed information. This refinement builds on the results generated by the IEB and AB blocks. The output of the VRM is defined as follows:

$$\mathbf{VRM}_{out} = \text{Sigmoid}(\mathbf{W}_s * \mathbf{VRM}_{in}) \quad (19)$$

where \mathbf{W}_s is a learnable matrix. The VRM enables additional processing of the features obtained from previous modules, optimizing the visual quality of the resulting images.

3.2.4. Contrast Correction Module

The Contrast Correction Module (CCM) aims to improve the contrast of images processed earlier by the Visual Refinement Module (VRM). Its primary objective is to enhance the visual quality of contrast, ensuring that colors in underwater environments appear more vivid and realistic. The CCM employs the algorithm outlined in [44], starting with the input image \mathbf{CCM}_{in} , which is processed using the Probability Density Function of a Standard Normal Distribution (PDF-SND). This process is mathematically expressed as:

$$\phi = \frac{1}{\sqrt{2\pi}} \exp\left(-\frac{1}{2} \cdot (\mathbf{CCM}_{in})^2\right) \quad (20)$$

where ϕ represents the processed image resulting from the PDF-SND transformation. Subsequently, the same input image, \mathbf{CCM}_{in} , undergoes further enhancement using the Softplus function, denoted as ψ , which is defined as:

$$\psi = \log(1 + \exp(\mathbf{CCM}_{in})) \quad (21)$$

Once ϕ and ψ are computed, the module applies a Logarithmic Image Processing (LIP) model to combine these components. The LIP model is described by the equation:

$$\mathbf{I}' = \sqrt{\phi + \psi + \phi \cdot \psi} \quad (22)$$

where \mathbf{I}' denotes the intermediate image generated by this model. The final step in the CCM involves applying a gamma-controlled normalization function to produce the contrast-enhanced image. This step is defined as:

$$\mathbf{CCM}_{out} = \left(\frac{\mathbf{I}' - \mathbf{I}'_{min}}{\mathbf{I}'_{max} - \mathbf{I}'_{min}}\right)^\gamma \quad (23)$$

where \mathbf{CCM}_{out} is the final output image with enhanced contrast, γ is the gamma correction factor, a parameter used to control the intensity of contrast enhancement, \mathbf{I}'_{min} is the minimum intensity value of the intermediate image \mathbf{I}' , and \mathbf{I}'_{max} is the maximum intensity value of \mathbf{I}' .

By systematically applying these steps, the CCM effectively enhances underwater images captured under non-uniform illumination conditions. The result is a more balanced color distribution and improved visibility of fine details, significantly contributing to the visual enhancement of submarine imagery.

3.3. Objective Function

To improve the visual quality of underwater images with non-uniform illumination, the total loss function, denoted as $\mathcal{L}_{UNIR-Net}$, is formulated as a combination of three complementary components: contrast loss (\mathcal{L}_c), structural loss (\mathcal{L}_s), and perceptual loss (\mathcal{L}_p). This design ensures that the enhanced images exhibit improved contrast, retain essential structural details, and maintain perceptual consistency with reference images. The total loss function $\mathcal{L}_{UNIR-Net}$ is defined as follows:

$$\mathcal{L}_{UNIR-Net} = \mathcal{L}_c + \mathcal{L}_s + \mathcal{L}_p \quad (24)$$

Contrast Loss. The contrast loss \mathcal{L}_c evaluates the consistency of brightness and contrast between the enhanced image \hat{y} and the reference image y . This term employs the L_1 distance, which measures the average absolute difference between the two sets of pixels over a total of N pixels. Its primary objective is to ensure that the brightness and contrast characteristics of the generated image align with those of the reference. The loss is calculated using the following expression:

$$\mathcal{L}_c = \frac{1}{N} \sum_{i=1}^N \|y - \hat{y}\|_1 \quad (25)$$

Structural Loss. The structural loss evaluates the Structural Similarity Index (SSIM) [45] between the enhanced image \hat{y} and the reference image y . This measure penalizes structural discrepancies, aiming to preserve the spatial integrity of the image. It is calculated using the following formula:

$$\mathcal{L}_s = 1 - \frac{(2\mu_{\hat{y}}\mu_y + c_1)(2\sigma_{\hat{y}y} + c_2)}{(\mu_{\hat{y}}^2 + \mu_y^2 + c_1)(\sigma_{\hat{y}}^2 + \sigma_y^2 + c_2)} \quad (26)$$

In this expression, $\mu_{\hat{y}}$ and μ_y represent the mean intensities of the enhanced and reference images, respectively. $\sigma_{\hat{y}}$ and σ_y are the variances of each image, and $\sigma_{\hat{y}y}$ is the covariance between both images. The constants c_1 and c_2 are used to stabilize the division calculation.

Perceptual Loss. The perceptual loss guarantees that the enhanced image \hat{y} closely resembles the reference image y in terms of visual appearance by comparing high-level features extracted using a pre-trained network, specifically the VGG network[46, 47]. The perceptual loss is defined as:

$$\mathcal{L}_p = \frac{1}{N} \sum_{i=1}^N \frac{1}{C_j H_j W_j} \|\phi_j(\hat{y}) - \phi_j(y)\|_2^2 \quad (27)$$

where, ϕ_j represents the feature map of the j -th layer of the pre-trained network, and C_j , H_j , and W_j are the channel, height, and width dimensions, respectively.

4. Experiments and Analysis

This section delves into the datasets utilized for performance evaluation, detailing their relevance and specific challenges related to underwater images with non-uniform illumination. It outlines the evaluation framework, including the metrics selected to rigorously benchmark the proposed method and the comparative approaches employed. Additionally, the training process of UNIR-Net is thoroughly described, emphasizing the steps taken to optimize its performance. A comprehensive analysis of the results is provided, highlighting both quantitative and qualitative aspects, as well as comparisons across multiple datasets tailored to address the complexities of non-uniform lighting. The section also examines ablation studies to uncover the contributions of individual components, evaluates computational efficiency, and explores the broader implications of using the method as a preprocessing step for downstream tasks in underwater image analysis.

4.1. Experiment settings

4.1.1. Implementation Details

The training of UNIR-Net leverages the PyTorch framework [48], a widely adopted open-source library designed for building and optimizing complex neural network architectures. The experiments are conducted on a system equipped with an NVIDIA RTX 3060 GPU, an Intel Core i5-12400F CPU running at 2.50 GHz, and 16 GB of RAM, ensuring a robust computational setup. For the training phase, a total of 2,786 images from the PUNI dataset are utilized, while an additional 491 images are allocated exclusively for testing purposes. To facilitate learning, the training process uses 128x128 image patches and processes mini-batches of 8 images. The model is trained over 100 epochs using the Adam optimizer [49], with an initial learning rate set to $1e - 4$. This configuration ensures efficient convergence and optimization tailored to the unique challenges posed by the PUNI dataset.

4.1.2. Benchmark Datasets

To comprehensively evaluate the proposed method, two datasets are utilized: the PUNI test set and a real-world unpaired dataset named Non-Uniform Illumination Dataset (NUID) [7]. The PUNI test set, comprising 491 images, enables performance assessments using both full-reference and non-reference metrics, ensuring a detailed evaluation. However, recognizing the limitations posed by the unavailability of training codes for some state-of-the-art methods, a secondary evaluation is conducted using the NUID dataset to ensure a more equitable comparison. NUID, a large-scale dataset tailored for enhancing underwater images with non-uniform illumination, includes 925 real-world images sourced from a variety of collections: UIEB [36] (32 images), EUVP [35] (256 images), OceanDark [50] (21 images), Google Image (96 images), and Nature Footage (520 images). By incorporating this diverse dataset, the evaluation framework ensures fairness and better reflects real-world conditions, offering a robust comparison of UNIR-Net’s capabilities against other state-of-the-art approaches.

4.1.3. Evaluation Metrics

The evaluation process incorporates a combination of Full-reference Image Quality Assessment (FIQA) and No-reference Image Quality Assessment (NIQA) metrics to comprehensively analyze the performance of the proposed method. FIQA metrics, such as Peak Signal-to-Noise Ratio (PSNR)[45], Structural Similarity Index Measure (SSIM)[45], Universal Quality Index (UQI)[51], Learned Perceptual Image Patch Similarity (LPIPS)[52], and DeltaE [53], are employed to quantify image quality in terms of pixel accuracy, structural fidelity, perceptual similarity, and color consistency. These metrics evaluate reconstructed images against their ground truth.

Complementing this, NIQA metrics are utilized to assess image quality without requiring reference images, focusing on aspects critical to underwater scenarios. This includes Underwater Color Image Quality Evaluation (UCIQE)[54], tailored specifically for underwater environments; Fog Aware Density Evaluator (FADE)[55], for analyzing fog-related image degradation; No-reference Image Quality Metric for Contrast (NIQMC)[56], which measures contrast performance; and Multi-Scale Image Quality Transformer (MUSIQ)[57], leveraging multi-scale features for a robust assessment. By integrating these diverse metrics, the evaluation framework ensures a thorough comparison of the proposed method with state-of-the-art approaches, capturing both objective quality and perceptual improvements.

4.1.4. Comparison Methods

To assess the performance of UNIR-Net, a comprehensive comparison was conducted with multiple state-of-the-art methods. Specifically, 11 techniques focusing on the enhancement of underwater images were considered: UNTV [23], UWnet [29], ACDC [2], MMLE [25], TCTL-Net [3], ICSP [7], PCDE [26], UDAformer [4], HFM [28], LENet [32], and SMDR-IS [33]. Additionally, 5 in-air methods aimed at enhancing low-light images were included in the evaluation: LIME (Guo et al., 2016)[14], DUAL (Zhang et al., 2019)[15], Zero-DCE [16], GACA [17], and GCP [18]. These methods enable a comprehensive comparison of the proposed method with state-of-the-art techniques, ensuring a robust evaluation in scenarios with non-uniform illumination.

4.2. Evaluation Results and Discussion

4.2.1. Qualitative Results

The qualitative evaluation examines images from the PUNI and NUID datasets, emphasizing the performance of various methods under non-uniform illumination conditions. In Fig. 6, corresponding to the PUNI dataset, methods such as UNTV, GACA, and UWNet exhibit noticeable color distortions. Conversely, approaches like LIME, DUAL, Zero-DCE, and GCP enhance illumination but produce softer edges, leading to a blurred appearance. Techniques such as MMLE, PCDE, HFM, SMDR-IS, and UDAformer leave dark regions in the images, resulting in uneven tonal distribution. While TCTL-Net, ACDC, and LENet improve illumination, they generate muted colors and lead to a loss of detail. Among the evaluated methods, ICSP and the proposed UNIR-Net excel in enhancing illumination and edge definition. However, the proposed UNIR-Net surpasses ICSP by achieving a superior balance in color representation and edge sharpness.

In Fig. 7, corresponding to the NUID dataset, methods like LIME, DUAL, and GCP successfully enhance illumination but oversaturate green tones. In contrast, UNTV, UWNet, and HFM improve color accuracy while failing to sufficiently enhance illumination. Zero-DCE introduces a haze effect, while PCDE, MMLE, and SMDR-IS produce images with persistent dark regions. Techniques such as LENet, GACA, TCTL-Net, and ACDC enhance illumination, yet the resulting colors appear dull. ICSP effectively highlights edges but offers limited illumination enhancement. UDAformer strikes a balance between illumination and color but sacrifices edge definition. In comparison, the proposed UNIR-Net consistently produces well-illuminated images with vibrant colors and sharp edges, distinguishing itself from other methods.

The qualitative analysis confirms that the proposed UNIR-Net delivers outstanding performance across diverse underwater scenarios characterized by challenging lighting conditions. Its key strengths include effective illumination enhancement, preservation of vibrant colors, and precise edge definition critical attributes for the visual restoration of underwater images impacted by non-uniform illumination.

4.2.2. Quantitative Results

Table 1 presents a quantitative evaluation of the PUNI dataset using various image quality metrics. The proposed method, UNIR-Net, demonstrates superior performance by achieving the highest values in PSNR, SSIM, and UQI,

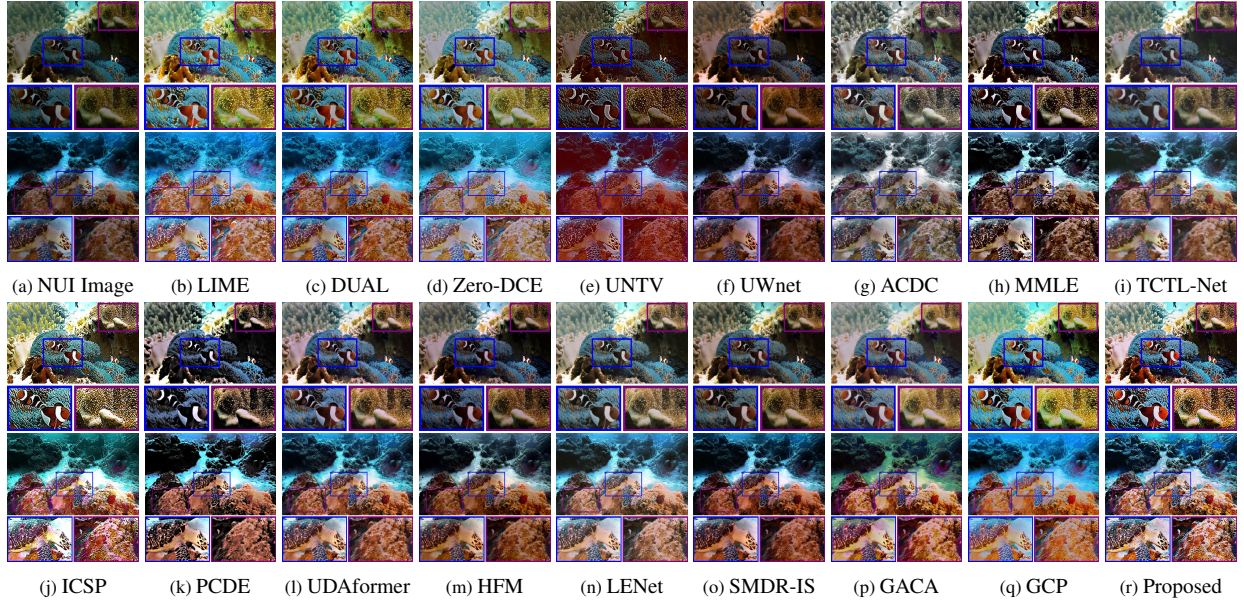


Figure 6: Visual comparison of methods for enhancing non-illumination underwater images on PUNI dataset.

Table 1: Quantitative Comparison on the PUNI Dataset.

Method	Year	FIQA					NIQA			
		PSNR \uparrow	SSIM \uparrow	UQI \uparrow	LPIPS \downarrow	DeltaE \downarrow	UCIQE \uparrow	FADE \downarrow	NIQMC \uparrow	MUSIQ \uparrow
LIME [14]	2016	12.9367	0.6547	0.7541	0.3753	26.2524	0.6612	0.2308	5.2460	66.7589
DUAL [15]	2019	12.9360	0.6438	0.7451	0.3809	24.9899	0.6403	0.2212	5.0528	67.6927
Zero-DCE [16]	2020	13.3474	0.6249	0.7745	0.4109	25.1052	0.6109	0.2655	4.9048	67.8858
UNTV [23]	2021	10.4148	0.4045	0.5619	0.3176	33.8359	0.6503	0.1572	4.9717	62.5657
UWnet [29]	2021	9.8603	0.3162	0.4581	0.5920	37.1908	0.5680	0.2945	4.2854	58.2181
ACDC [2]	2022	13.6405	0.5785	0.7954	0.4190	22.5252	0.6098	0.2773	5.4007	66.1372
MMLE [25]	2022	13.9459	0.6322	0.7019	0.2588	22.1338	0.6612	0.1868	5.2876	66.0242
TCTL-Net [3]	2023	12.6514	0.4649	0.7516	0.5790	24.9678	0.6188	0.3868	5.2356	56.5916
ICSP [7]	2023	13.6869	0.7042	0.7723	0.2418	21.1913	0.6820	0.1534	5.3652	65.6839
PCDE [26]	2023	12.1812	0.4795	0.5977	0.4273	28.4354	0.6556	0.1550	5.0770	62.7529
UDAformer [4]	2023	14.2730	0.6531	0.8211	0.3907	21.1077	0.6519	0.2362	5.4164	66.6605
HFM [28]	2024	11.8410	0.4530	0.6564	0.4353	26.9411	0.6227	0.2590	5.1111	64.1482
LENet [32]	2024	13.6257	0.5669	0.7913	0.4283	24.1685	0.6028	0.3749	5.1782	65.5047
SMDR-IS [33]	2024	11.7681	0.5037	0.6333	0.4327	28.8656	0.6148	0.2523	4.8751	65.3956
GACA [17]	2024	12.6868	0.4677	0.7686	0.4907	25.4277	0.6116	0.3842	5.1878	66.3268
GCP [18]	2024	14.1003	0.6833	0.7786	0.3137	22.3167	0.6765	0.2212	5.3022	68.2599
UNIR-Net (Proposed)	2025	19.7054	0.8771	0.8903	0.0667	11.0012	0.7082	0.1466	5.5852	67.6252

along with the lowest values in LPIPS and DeltaE. This indicates that UNIR-Net produces images with greater fidelity to the original data and enhanced visual perception. In the NIQA metrics, UNIR-Net also excels, achieving the highest values in UCIQE and NIQMC, as well as the lowest value in FADE. This highlights its ability to generate more natural images with better visual balance. However, in the MUSIQ metric, the GCP method ranks first.

Meanwhile, Tables 2 and 3 detail the results obtained on the NUID dataset, evaluated using UCIQE, FADE, NIQMC, and MUSIQ metrics. The metrics were calculated for different subsets of the dataset, including Enhanced Underwater Visual Perception (EUVP), Google Image (GI), Nature Footage (NF), OceanDark (OD), and Underwater Image Enhancement Benchmark (UIEB), as well as the overall average. In this evaluation, UNIR-Net consistently shows the best average performance, standing out with the highest average values in UCIQE, NIQMC, and MUSIQ, and the lowest average value in FADE. This confirms that UNIR-Net not only enhances the visual quality of real-world underwater images but also preserves a natural appearance, significantly outperforming current state-of-the-art methods.

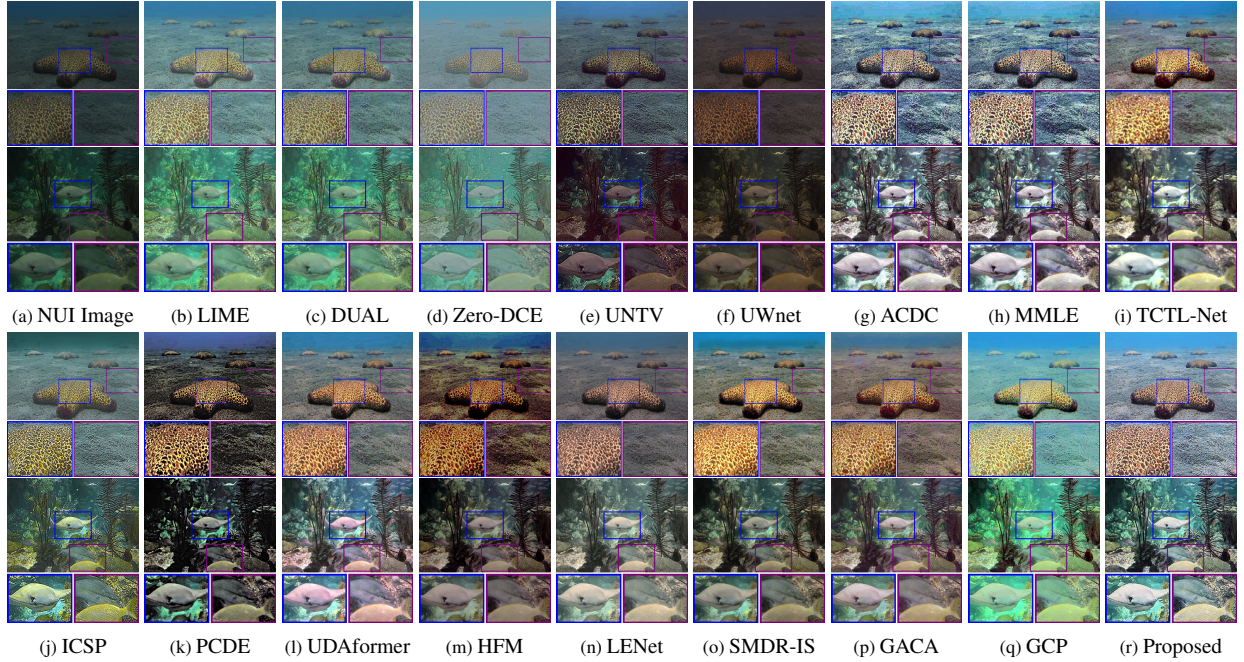


Figure 7: Visual comparison of methods for enhancing low illumination underwater images on NUID dataset.

Table 2: Comparison results on NUID underwater image dataset in terms of UCIQE and FADEJ.

Method	UCIQE \uparrow						FADEJ					
	EUVP	GI	NF	OD	UIEB	Average	EUVP	GI	NF	OD	UIEB	Average
LIME [14]	0.5779	0.5413	0.5429	0.5383	0.5557	0.5512	0.2860	0.7051	1.0198	1.1744	0.6798	0.7730
DUAL [15]	0.5886	0.5478	0.5344	0.5525	0.5644	0.5575	0.2502	0.5962	0.8857	0.9188	0.5941	0.6490
Zero-DCE [16]	0.5330	0.4801	0.5073	0.4851	0.5053	0.5022	0.3041	0.9042	1.1857	1.5491	0.7806	0.9447
UNTV [23]	0.6270	0.6015	0.5581	0.5264	0.5947	0.5815	0.1941	0.4732	0.6159	0.8184	0.4816	0.5166
UWnet [29]	0.5801	0.5484	0.5084	0.5715	0.5572	0.5531	0.3520	0.8651	1.1000	1.2336	0.8571	0.8816
ACDC [2]	0.5769	0.5604	0.5651	0.5315	0.5713	0.5610	0.3061	0.6949	1.3274	1.1725	0.7273	0.8456
MMLE [25]	0.6224	0.6049	0.5833	0.5660	0.6095	0.5972	0.1978	0.5162	0.7549	0.8515	0.4535	0.5548
TCTL-Net [3]	0.5944	0.5915	0.5798	0.5437	0.6128	0.5844	0.4635	0.8790	1.4949	1.7122	0.8383	1.0776
ICSP [7]	0.6471	0.6035	0.5815	0.5857	0.6205	0.6077	0.1883	0.4263	0.7367	0.9540	0.3949	0.5400
PCDE [26]	0.6288	0.6127	0.5891	0.5670	0.6201	0.6035	0.1593	0.5398	0.5552	0.9016	0.3817	0.5075
UDAformer [4]	0.6225	0.6059	0.5765	0.5767	0.6271	0.6017	0.2888	0.6084	1.0143	1.1073	0.6145	0.7267
HFM [28]	0.6106	0.5942	0.5640	0.5686	0.5970	0.5869	0.3073	0.7005	1.1409	1.3086	0.7484	0.8411
LENet [32]	0.5949	0.5818	0.5304	0.5659	0.5937	0.5733	0.3850	0.7831	1.7562	1.4539	0.8541	1.0465
SMDR-IS [33]	0.6130	0.5926	0.5628	0.5696	0.6083	0.5893	0.2910	0.5457	0.9054	0.9198	0.7146	0.6753
GACA [17]	0.5877	0.5819	0.5838	0.5447	0.6009	0.5798	0.3875	0.7703	1.3253	1.5360	0.7181	0.9474
GCP [18]	0.6272	0.5964	0.6019	0.5762	0.6137	0.6031	0.2567	0.6198	0.8505	1.1737	0.6053	0.7012
UNIR-Net (Proposed)	0.6533	0.6232	0.6039	0.6001	0.6323	0.6225	0.1572	0.3085	0.6656	0.6363	0.3245	0.4184

These quantitative results underscore the effectiveness of the proposed method, both in terms of fidelity to the original information and the naturalness of the enhanced images, establishing it as a robust solution for improving underwater images with non-uniform illumination.

4.2.3. Comparison of training datasets in UNIR-Net

To highlight the significance of the PUNI dataset in training, the proposed UNIR-Net method trains on various datasets. For in-air low-light images, the Low-Light (LOL)[37] and MIT-Adobe FiveK[39] datasets serve as references, while for underwater low-light images, the Low-light Underwater Image Enhancement (LUIE) [30] dataset provides the necessary data.

LOL dataset includes 500 paired images with varying exposure times and ISO settings, illustrating both low and normal lighting conditions. Similarly, the MIT-Adobe FiveK dataset presents 5000 DSLR images, offering diverse

Table 3: Comparison results on NUID underwater image dataset in terms of NIQMC and MUSIQ.

Method	NIQMC \uparrow						MUSIQ \uparrow					
	EUVP	GI	NF	OD	UIEB	Average	EUVP	GI	NF	OD	UIEB	Average
LIME [14]	5.0359	4.7154	4.3958	5.1076	4.8254	4.8160	58.7525	53.7518	34.5371	44.1840	48.0657	47.8582
DUAL [15]	4.9704	4.6382	4.2566	5.0949	4.7295	4.7379	59.2917	54.3826	34.3405	47.1085	48.9220	48.8091
Zero-DCE [16]	4.6816	4.0521	4.0711	4.6244	4.2000	4.3258	61.0729	56.1542	38.7419	47.7606	52.7634	51.2986
UNTV [23]	4.9137	4.8215	4.3360	4.8374	4.6429	4.7103	57.7946	52.7507	37.9192	48.8997	51.8534	49.8435
UWnet [29]	4.6532	4.3660	3.7366	4.9869	4.4004	4.4286	55.6179	48.3772	32.6250	47.1962	47.4309	46.2494
ACDC [2]	5.2697	5.2990	4.9161	5.3163	5.3108	5.2224	57.7228	50.5946	31.5843	45.6607	47.0116	46.5148
MMLE [25]	5.1769	5.3519	4.8767	5.3660	5.3106	5.2164	59.8614	54.0019	34.9565	48.6503	50.7224	49.6385
TCTL-Net [3]	5.1747	5.1455	4.8806	5.1260	5.2888	5.1231	52.0720	41.1017	34.8615	36.0238	40.2606	40.8639
ICSP [7]	5.2242	5.0117	4.5138	5.1488	5.2406	5.0278	59.8850	52.3104	35.4520	45.3621	51.7898	48.9599
PCDE [26]	4.9899	5.0996	4.7900	5.4514	5.1401	5.0942	56.6199	52.0433	35.4325	44.8043	49.7388	47.7278
UDAformer [4]	5.3526	5.2446	4.9392	5.5604	5.3755	5.2945	58.4523	54.3923	34.9949	44.1347	50.6314	48.5211
HFM [28]	5.3131	5.2834	4.7723	5.4502	5.2289	5.2096	56.1166	50.0688	33.4501	44.2613	47.9797	46.3753
LENet [32]	5.2623	5.1139	4.6004	5.4952	5.2439	5.1431	58.4278	54.4434	35.8024	42.2083	49.7863	48.1336
SMDR-IS [33]	5.1165	5.0517	4.6384	5.3784	5.2061	5.0782	57.5129	52.9491	33.3865	43.0757	48.2745	47.0398
GACA [17]	5.0149	5.0213	5.0587	5.2346	5.2539	5.1167	58.6684	54.1030	35.2923	42.6933	49.6183	48.0751
GCP [18]	5.3321	5.1731	4.9009	5.4067	5.2463	5.2118	59.2625	53.0948	34.0865	42.7211	46.8959	47.2122
UNIR-Net (Proposed)	5.4463	5.3039	5.0367	5.5034	5.4504	5.3481	61.2277	58.4932	35.8605	52.3809	49.8281	51.5581

scenarios of low-light environments. In the underwater domain, the LUIE dataset generates 2524 paired images derived from 362 underwater scenes, targeting the specific challenges posed by low-light conditions in underwater environments.

Figure 8 presents a visual comparison of the results obtained by training UNIR-Net with the different datasets mentioned. In this comparison, it can be seen that the LOL dataset significantly improves lighting and color; however, it does not achieve a notable improvement in the image edges and shows a slight haze effect. On the other hand, the MIT dataset enhances lighting but at the cost of leaving some dark areas in the enhanced images. The LUIE dataset introduces color distortions by producing enhanced images with unusual hues. In contrast, the use of the PUNI dataset provides the best visual results, significantly improving lighting, maintaining natural color, and achieving better edge detail compared to the other datasets.

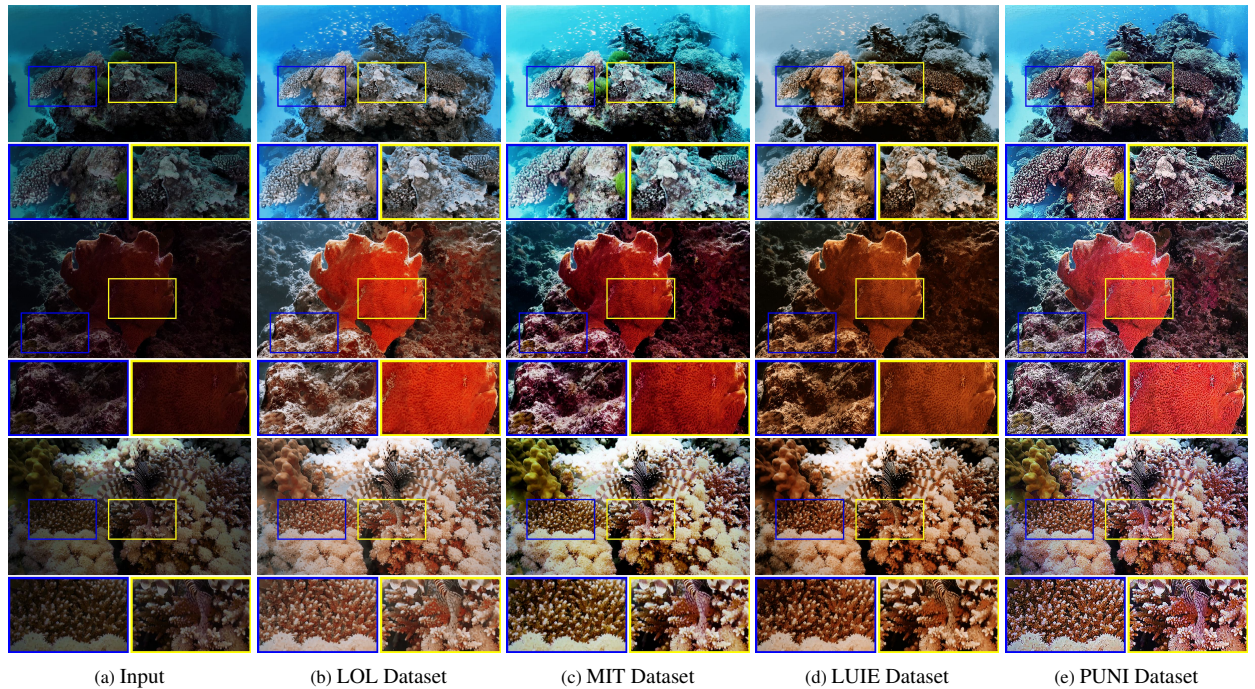


Figure 8: Comparison of training datasets in UNIR-Net.

4.3. Additional Analyses

4.3.1. Ablation Study

In this section, the contribution of the different components of the model is evaluated through an ablation study. This quantitative analysis examines the impact of removing key parts of the architecture during the synthesis process of underwater images with non-uniform illumination, using the NUID dataset as a reference. Metrics such as UCIQE and NIQMC were employed to ensure a comprehensive evaluation of color fidelity and image quality under varying illumination conditions. The results for the PUNI model are presented in Table 4, while the outcomes for the UNIR-Net model, after the removal of specific components, are detailed in Table 5.

Table 4: Quantitative results of the PUNI dataset synthesis evaluated under different ablation scenarios.

Model	Components		Metrics	
	Mask	Sharper	UCIQE \uparrow	NIQMC \uparrow
Model w/o Mask	×	✓	0.6112	5.2866
Model w/o Sharper	✓	×	0.6064	5.2649
Full Model	✓	✓	0.6225	5.3481

Table 5: Quantitative results of the UNIR-Net model under different ablation scenarios.

Model	Components			Metrics	
	Core	VRM	CCM	UCIQE \uparrow	NIQMC \uparrow
Model w/o Core and VRM	×	×	✓	0.5611	4.5416
Model w/o VRM	✓	×	✓	0.5270	4.2766
Model w/o CCM	✓	✓	×	0.6123	5.2927
Full Model	✓	✓	✓	0.6225	5.3481

Table 4 details the impact of removing individual components, such as the mask and sharper synthesis. When the mask is removed, the UCIQE and NIQMC values significantly decrease, reaching 0.6112 and 5.2866, respectively. Similarly, suppressing the sharpening also negatively impacts performance, with UCIQE and NIQMC values dropping to 0.6064 and 5.2649, respectively. In contrast, the full model, which integrates both the mask and the sharpening synthesis, achieves the best results with a UCIQE of 0.6225 and a NIQMC of 5.3481. Figure 9 illustrates visual results showing that including all model components produces the most visually enhanced images.

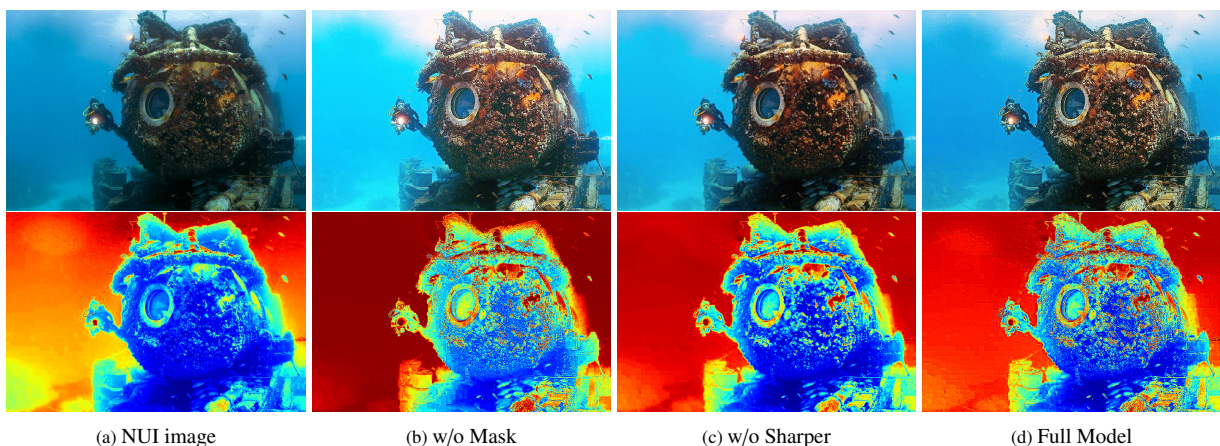


Figure 9: Comparison of dataset versions generated with different components.

On the other hand, Table 5 evaluates the impact of removing additional components, such as the Core, VRM, and CCM. Jointly removing the Core and VRM severely affects performance, resulting in UCIQE and NIQMC scores

of 0.5611 and 4.5416, respectively. Furthermore, the removal of only the VRM leads to even lower performance, highlighting the importance of this module. Finally, excluding the CCM reduces the metrics to a UCIQE of 0.6123 and an NIQMC of 5.2927. In all cases, the Full Model demonstrates superior performance, achieving a UCIQE of 0.6225 and an NIQMC of 5.3481.

These results highlight the significance of each component within the proposed architecture and the data synthesis process. Moreover, they validate the effectiveness of the proposed design in improving both visual quality and quantitative metrics for underwater images with non-uniform illumination.

4.3.2. Refining high-level vision processing

In marine vision applications, particularly in semantic segmentation of underwater images, the UNIR-Net method emerges as an effective solution for preprocessing these types of images. To qualitatively evaluate the impact of UNIR-Net in comparison with various state-of-the-art methods, the SAM [42] is utilized. This model automatically generates semantic segmentation masks in different environments.

Figure 10 illustrates an example of a low-light input image and the results obtained with other methods. In this comparison, techniques such as LIME, DUAL, Zero-DCE, GCP, LENet, UDAformer, ACDC, and GACA achieve significant improvements in image illumination. However, when these processed images are used for this type of segmentation, they encounter difficulties in detecting fish due to the loss of specific details during the enhancement process.

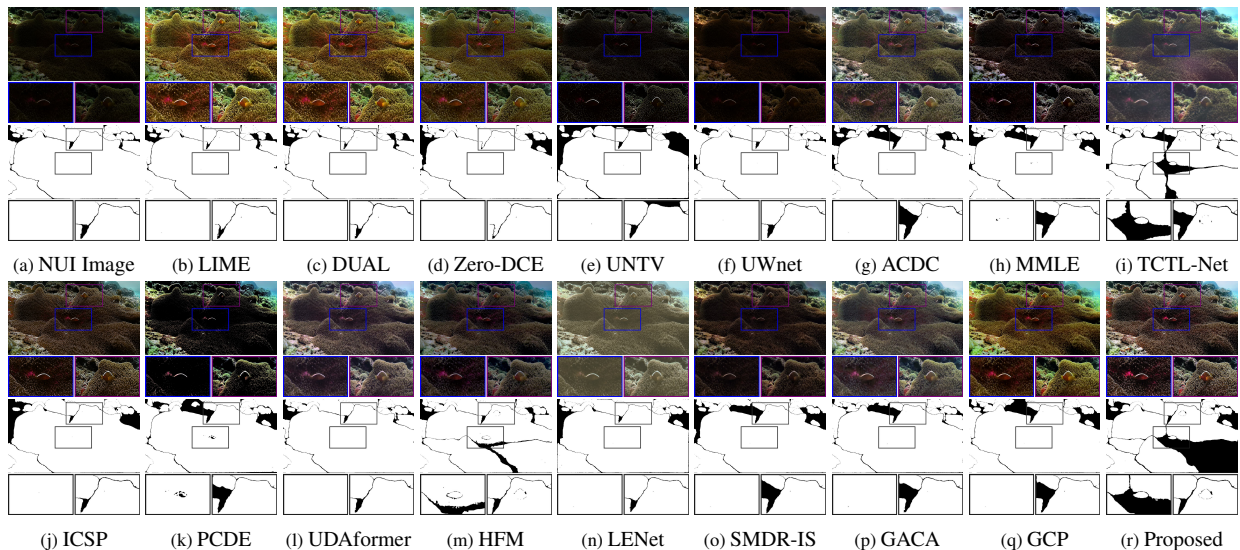


Figure 10: Comparisons of different enhancement methods results for later segmentation in images with non-uniform illumination.

In contrast, methods such as UNTV, UWNNet, MMLE, PCDE, ICSP, and SMDR-IS do not produce notable improvements in illumination, resulting in segmentation quality comparable to that of the original image, without correctly identifying the fish present in the scene. On the other hand, methods like TCTL-Net, HFM, and the proposed UNIR-Net excel by providing more accurate segmentation of the fish.

These findings underscore the importance of employing advanced underwater image enhancement techniques as a preliminary stage for high-level computer vision tasks. Improving the visual quality of the images enables clearer and more precise segmentation of marine fauna, which is essential for advanced computer vision applications in challenging underwater environments.

4.3.3. Computational cost comparison

The computational cost of the proposed UNIR-Net model is evaluated and compared with state-of-the-art methods under two distinct scenarios: GPU-based and CPU-based implementations. For the evaluation, 30 images of $1280 \times$

720 resolution are used. Tables 6 and 7 provide detailed comparisons in terms of inference speed, parameter count, FLOPs, memory usage, and platform implementation.

Table 6 highlights the efficiency of various GPU-based methods, including deep learning models. Among the models, Zero-DCE exhibits the fastest inference speed (0.2287 s) and the smallest number of parameters (0.08M), making it highly efficient for lightweight applications. LENet, with the lowest FLOPs (9.70G), achieves computational efficiency but trades off a slightly slower inference speed. The proposed UNIR-Net, with an inference speed of 0.3297 s, 0.34M parameters, and 311.56G FLOPs, provides a balanced performance between computational efficiency and model complexity. However, UNIR-Net requires slightly more memory (2,085.57 MB) compared to some lightweight models. Notably, UDAformer, while achieving competitive results in performance, demonstrates a high computational cost with 1.7358 s inference time and 584.90G FLOPs, showcasing the trade-offs between accuracy and efficiency in transformer-based approaches.

Table 6: Comparison of computational cost for GPU-based methods.

Method	Year	Inference Speed (s) ↓	# Parameters ↓	FLOPs (G) ↓	Memory Usage (MB) ↓	Platform
Zero-DCE [16]	2020	0.2287	0.08 (M)	72.99	1,222.23	PyTorch
UWnet [29]	2021	0.2860	0.22 (M)	304.17	1,364.53	PyTorch
TCTL-Net [3]	2023	0.2371	99.72 (M)	56.62	765.45	PyTorch
UDAformer [4]	2023	1.7358	9.59 (M)	584.90	3,880.11	PyTorch
LENet [32]	2024	0.2596	0.01 (M)	9.70	1,543.99	PyTorch
SMDR-IS [33]	2024	0.5575	12.25 (M)	724.78	2,161.63	PyTorch
GACA [17]	2024	0.6168	5.74 (M)	652.26	1,488.04	PyTorch
UNIR-Net (Proposed)	2025	0.3297	0.34 (M)	311.56	2,085.57	PyTorch

Table 7 presents a comparison of CPU-based methods, focusing on traditional algorithms and optimization techniques. In this category, GCP outperforms other methods with an impressive inference speed of 0.2375 s, making it ideal for real-time or resource-constrained environments. The proposed UNIR-Net demonstrates a moderate CPU inference time of 8.7085 s, which, while not the fastest, remains competitive among recent learning-based models implemented on CPUs. Classical methods such as LIME and DUAL show significantly higher inference times (11.0941 s and 22.3193 s, respectively), reflecting their reliance on iterative optimization techniques. Meanwhile, hybrid approaches like MMLE and ACDC, implemented in Matlab, achieve relatively faster processing but still lag behind UNIR-Net in flexibility and scalability for GPU environments.

Table 7: Comparison of computational cost for CPU-based methods.

Method	Year	Inference Speed (s) ↓	Platform
LIME [14]	2016	11.0941	Python
DUAL [15]	2019	22.3193	Python
UNTV [23]	2021	21.4268	Matlab
ACDC [2]	2022	2.1339	Matlab
MMLE [25]	2022	0.9006	Matlab
ICSP [7]	2023	1.4530	Matlab
PCDE [26]	2023	3.0262	Matlab
HFM [28]	2024	3.2908	Matlab
GCP [18]	2024	0.2375	Python
UNIR-Net (Proposed)	2025	8.7085	Pytorch

The results indicate that UNIR-Net is optimized for GPU acceleration, where it strikes a balance between inference speed, computational resources, and memory usage. While the CPU-based implementation could be further optimized, the focus remains on leveraging GPU efficiency to handle the complex task of underwater image enhancement under non-uniform illumination.

5. Conclusion

This article introduces UNIR-Net, an architecture specifically designed to address the challenges of limited visibility in underwater environments with non-uniform illumination. This method combines Illumination Enhancement

and Attention blocks with Visual Refinement and Contrast Correction modules, effectively preserving both the visual quality of images and maintaining appropriate illumination and edge detail.

Additionally, PUNI, a synthetic dataset, is presented, developed specifically to study and resolve issues related to uneven lighting conditions in underwater environments. Experimental results, both qualitative and quantitative, demonstrate that UNIR-Net outperforms state-of-the-art methods across various metrics, excelling in FIQA metrics while achieving competitive performance in the MUSIQ metric. In the large-scale unpaired real-world dataset NUID, the proposed method shows superior performance, attaining a consistently high average value across all evaluated subsets. Furthermore, in practical applications, UNIR-Net has a significant impact on high-level tasks such as marine fauna segmentation, thanks to its ability to enhance visual details and edges. In terms of computational cost, although UNIR-Net is not the most efficient method in resource usage, its balance between visual quality and computational consumption positions it favorably compared to lighter alternatives that produce inferior visual results.

As future research directions, expanding the PUNI dataset is proposed to incorporate a greater diversity of characteristics typical of underwater environments with non-uniform illumination. Additionally, optimizing the UNIR-Net architecture aims to further reduce its computational cost without compromising performance.

6. Acknowledgments

This work is supported by the Zhejiang Provincial Natural Science Foundation of China (No.LY24F020004, No.LZ23F020004), the Zhejiang Gongshang University "Digital+" Disciplinary Construction Management Project (No.SZJ2022B016) and the University of Guadalajara.

References

- [1] X. Cong, Y. Zhao, J. Gui, J. Hou, D. Tao, A Comprehensive Survey on Underwater Image Enhancement Based on Deep Learning, arXiv preprint arXiv:2405.19684 (2024).
- [2] W. Zhang, Y. Wang, C. Li, Underwater Image Enhancement by Attenuated Color Channel Correction and Detail Preserved Contrast Enhancement, *IEEE Journal of Oceanic Engineering* 47 (3) (2022) 718–735.
- [3] K. Li, H. Fan, Q. Qi, C. Yan, K. Sun, Q. J. Wu, TCTL-Net: Template-Free Color Transfer Learning for Self-Attention-Driven Underwater Image Enhancement, *IEEE Transactions on Circuits and Systems for Video Technology* 34 (6) (2023) 4682–4697.
- [4] Z. Shen, H. Xu, T. Luo, Y. Song, Z. He, UDAformer: Underwater Image Enhancement Based on Dual Attention Transformer, *Computers & Graphics* 111 (2023) 77–88.
- [5] T. P. Marques, A. B. Albu, L2UWE: A Framework for the Efficient Enhancement of Low-Light Underwater Images Using Local Contrast and Multi-Scale Fusion, in: *Proceedings of the IEEE/CVF Conference on Computer Vision and Pattern Recognition, IEEE/CVF, Virtual, 2020*, pp. 538–539.
- [6] W. Zhang, W. Liu, L. Li, H. Jiao, Y. Li, L. Guo, J. Xu, A Framework for the Efficient Enhancement of Non-Uniform Illumination Underwater Images Using Convolutional Neural Network, *Computers & Graphics* 112 (2023) 60–71.
- [7] G. Hou, N. Li, P. Zhuang, K. Li, H. Sun, C. Li, Non-Uniform Illumination Underwater Image Restoration via Illumination Channel Sparsity Prior, *IEEE Transactions on Circuits and Systems for Video Technology* 34 (2) (2023) 799–814.
- [8] W. Zhao, S. Rong, C. Feng, B. He, PSNet: A Non-Uniform Illumination Correction Method for Underwater Images Based on Pseudo-Siamese Network, *Knowledge-Based Systems* (2024) 112780.
- [9] A. Sahoo, S. K. Dwivedy, P. Robi, Advancements in the Field of Autonomous Underwater Vehicle, *Ocean Engineering* 181 (2019) 145–160.
- [10] K. Hasan, S. Ahmad, A. F. Liaf, M. Karimi, T. Ahmed, M. A. Shawon, S. Mekhilef, Oceanic Challenges to Technological Solutions: A Review of Autonomous Underwater Vehicle Path Technologies in Biomimicry, Control, Navigation and Sensing, *IEEE Access* 12 (2024).
- [11] J. He, Introduction Remote-operated Underwater Vehicle for Inspection of Underwater Structure, *Highlights in Science, Engineering and Technology* 97 (2024) 214–219.
- [12] S. Xu, M. Zhang, W. Song, H. Mei, Q. He, A. Liotta, A Systematic Review and Analysis of Deep Learning-Based Underwater Object Detection, *Neurocomputing* 527 (2023) 204–232.
- [13] A. Abdullah, T. Barua, R. Tibbetts, Z. Chen, M. J. Islam, I. Rekleitis, CaveSeg: Deep Semantic Segmentation and Scene Parsing for Autonomous Underwater Cave Exploration, in: *Proceedings of the IEEE International Conference on Robotics and Automation, Yokohama, Japan, 2024*, pp. 3781–3788.
- [14] X. Guo, Y. Li, H. Ling, LIME: Low-Light Image Enhancement via Illumination Map Estimation, *IEEE Transactions on Image Processing* 26 (2) (2016) 982–993.
- [15] Q. Zhang, Y. Nie, W. S. Zheng, Dual Illumination Estimation for Robust Exposure Correction, *Computer Graphics Forum* 38 (2019) 243–252.
- [16] C. Guo, C. Li, J. Guo, et al., Zero-Reference Deep Curve Estimation for Low-Light Image Enhancement, in: *Proceedings of the IEEE/CVF Conference on Computer Vision and Pattern Recognition, IEEE/CVF, Virtual, 2020*, pp. 1780–1789.
- [17] Z. Yao, J.-N. Su, G. Fan, M. Gan, C. P. Chen, GACA: A Gradient-Aware and Contrastive-Adaptive Learning Framework for Low-Light Image Enhancement, *IEEE Transactions on Instrumentation and Measurement* 73 (2024) 1–14.
- [18] J. J. Jeon, J. Y. Park, I. K. Eom, Low-Light Image Enhancement Using Gamma Correction Prior in Mixed Color Spaces, *Pattern Recognition* 146 (2024) 110001.

- [19] E. Perez-Zarate, O. Ramos-Soto, E. Rodríguez-Esparza, G. Aguilar, LoLi-IEA: Low-Light Image Enhancement Algorithm, in: Proceedings of the SPIE Optical Engineering + Applications, SPIE, San Diego, USA, 2023, pp. 230–245.
- [20] E. Perez-Zarate, O. Ramos-Soto, C. Liu, D. Oliva, M. Perez-Cisneros, ALEN: An Adaptive Dual-Approach for Enhancing Uniform and Non-Uniform Low-Light Images, arXiv preprint arXiv:2407.19708 (2024).
- [21] X. Ji, X. Wang, N. Leng, L.-Y. Hao, H. Guo, Dual-Branch Underwater Image Enhancement Network via Multiscale Neighborhood Interaction Attention Learning, *Image and Vision Computing* 151 (2024) 105256.
- [22] J. Yuan, W. Cao, Z. Cai, B. Su, An Underwater Image Vision Enhancement Algorithm Based on Contour Bougie Morphology, *IEEE Transactions on Geoscience and Remote Sensing* 59 (10) (2020) 8117–8128.
- [23] J. Xie, G. Hou, G. Wang, Z. Pan, A Variational Framework for Underwater Image Dehazing and Deblurring, *IEEE Transactions on Circuits and Systems for Video Technology* 32 (6) (2021) 3514–3526.
- [24] P. Zhuang, J. Wu, F. Porikli, C. Li, Underwater Image Enhancement with Hyper-Laplacian Reflectance Priors, *IEEE Transactions on Image Processing* 31 (2022) 5442–5455.
- [25] W. Zhang, P. Zhuang, H.-H. Sun, G. Li, S. Kwong, C. Li, Underwater Image Enhancement via Minimal Color Loss and Locally Adaptive Contrast Enhancement, *IEEE Transactions on Image Processing* 31 (2022) 3997–4010.
- [26] W. Zhang, S. Jin, P. Zhuang, Z. Liang, C. Li, Underwater Image Enhancement via Piecewise Color Correction and Dual Prior Optimized Contrast Enhancement, *IEEE Signal Processing Letters* 30 (2023) 229–233.
- [27] W. Zhang, L. Zhou, P. Zhuang, G. Li, X. Pan, W. Zhao, C. Li, Underwater Image Enhancement via Weighted Wavelet Visual Perception Fusion, *IEEE Transactions on Circuits and Systems for Video Technology* 34 (4) (2023) 2469–2483.
- [28] S. An, L. Xu, I. Senior Member, Z. Deng, H. Zhang, HFM: A Hybrid Fusion Method for Underwater Image Enhancement, *Engineering Applications of Artificial Intelligence* 127 (2024) 107219.
- [29] A. Naik, A. Swarnakar, K. Mittal, Shallow-UWNet: Compressed Model for Underwater Image Enhancement (Student Abstract), in: Proceedings of the 35th AAAI Conference on Artificial Intelligence, AAAI, Virtual, 2021, pp. 15853–15854.
- [30] Y. Xie, Z. Yu, X. Yu, B. Zheng, Lighting the Darkness in the Sea: A Deep Learning Model for Underwater Image Enhancement, *Frontiers in Marine Science* 9 (2022) 921492.
- [31] J. Wen, J. Cui, Z. Zhao, R. Yan, Z. Gao, L. Dou, B. M. Chen, SyreaNet: A Physically Guided Underwater Image Enhancement Framework Integrating Synthetic and Real Images, in: Proceedings of the IEEE International Conference on Robotics and Automation, London, UK, 2023, pp. 5177–5183.
- [32] S. Zhang, S. Zhao, D. An, D. Li, R. Zhao, LiteEnhanceNet: A Lightweight Network for Real-Time Single Underwater Image Enhancement, *Expert Systems with Applications* 240 (2024) 122546.
- [33] D. Zhang, J. Zhou, C. Guo, W. Zhang, C. Li, Synergistic Multiscale Detail Refinement via Intrinsic Supervision for Underwater Image Enhancement, in: Proceedings of the 38th AAAI Conference on Artificial Intelligence, AAAI, Vancouver, Canada, 2024, pp. 7033–7041.
- [34] C. W. Park, I. K. Eom, Underwater Image Enhancement Using Adaptive Standardization and Normalization Networks, *Engineering Applications of Artificial Intelligence* 127 (2024) 107445.
- [35] M. J. Islam, Y. Xia, J. Sattar, Fast Underwater Image Enhancement for Improved Visual Perception, *IEEE Robotics and Automation Letters* 5 (2) (2020) 3227–3234.
- [36] C. Li, C. Guo, W. Ren, et al., An Underwater Image Enhancement Benchmark Dataset and Beyond, *IEEE Transactions on Image Processing* 29 (2019) 4376–4389.
- [37] C. Wei, W. Wang, W. Yang, et al., Deep Retinex Decomposition for Low-Light Enhancement, arXiv preprint arXiv:1808.04560 (2018).
- [38] J. Hai, Z. Xuan, R. Yang, Y. Hao, F. Zou, F. Lin, S. Han, R2RNet: Low-Light Image Enhancement via Real-Low to Real-Normal Network, *Journal of Visual Communication and Image Representation* 90 (2023) 103712.
- [39] V. Bychkovsky, S. Paris, E. Chan, F. Durand, Learning Photographic Global Tonal Adjustment with a Database of Input/Output Image Pairs, in: Proceedings of the IEEE Conference on Computer Vision and Pattern Recognition, IEEE, Colorado Springs, USA, 2011, pp. 97–104.
- [40] C. Liu, F. Wu, X. Wang, EFINet: Restoration for Low-Light Images via Enhancement-Fusion Iterative Network, *IEEE Transactions on Circuits and Systems for Video Technology* 32 (12) (2022) 8486–8499.
- [41] J. Wu, C. Liu, B. Li, Texture-Aware and Structure-Preserving Superpixel Segmentation, *Computers & Graphics* 94 (2021) 152–163.
- [42] A. Kirillov, E. Mintun, N. Ravi, H. Mao, C. Rolland, L. Gustafson, T. Xiao, S. Whitehead, A. C. Berg, W.-Y. Lo, et al., Segment Anything, in: Proceedings of the IEEE/CVF International Conference on Computer Vision, IEEE/CVF, Paris, France, 2023, pp. 4015–4026.
- [43] K. He, J. Sun, X. Tang, Guided Image Filtering, *IEEE Transactions on Pattern Analysis and Machine Intelligence* 35 (6) (2012) 1397–1409.
- [44] A. Albakri, Z. Al-Ameen, Rapid Contrast Enhancement Algorithm for Natural Contrast-Distorted Color Images, *AL-Rafidain Journal of Computer Sciences and Mathematics* 15 (2) (2021) 73–90.
- [45] Z. Wang, A. C. Bovik, H. R. Sheikh, et al., Image Quality Assessment: From Error Visibility to Structural Similarity, *IEEE Transactions on Image Processing* 13 (4) (2004) 600–612.
- [46] J. Johnson, A. Alahi, F. Li, Perceptual Losses for Real-Time Style Transfer and Super-Resolution, in: Proceedings of the 14th European Conference on Computer Vision, Springer, Amsterdam, The Netherlands, 2016, pp. 694–711.
- [47] K. Simonyan, A. Zisserman, Very Deep Convolutional Networks for Large-Scale Image Recognition, arXiv preprint arXiv:1409.1556 (2014).
- [48] A. Paszke, S. Gross, F. Massa, A. Lerer, J. Bradbury, G. Chanan, PyTorch: An Imperative Style, High-Performance Deep Learning Library, *Advances in Neural Information Processing Systems* 32 (2019) 8026–8037.
- [49] D. P. Kingma, J. Ba, Adam: A Method for Stochastic Optimization, arXiv preprint arXiv:1412.6980 (2014).
- [50] T. Porto Marques, A. Branzan Albu, M. Hoeberechts, A Contrast-Guided Approach for the Enhancement of Low-Lighting Underwater Images, *Journal of Imaging* 5 (10) (2019) 79.
- [51] Z. Wang, A. C. Bovik, A Universal Image Quality Index, *IEEE Signal Processing Letters* 9 (3) (2002) 81–84.
- [52] R. Zhang, P. Isola, A. A. Efros, E. Shechtman, O. Wang, The Unreasonable Effectiveness of Deep Features as a Perceptual Metric, in: Proceedings of the IEEE Conference on Computer Vision and Pattern Recognition, IEEE, Salt Lake City, USA, 2018, pp. 586–595.
- [53] H. Xu, X. Liu, H. Zhang, X. Wu, W. Zuo, Degraded Structure and Hue Guided Auxiliary Learning for Low-Light Image Enhancement, *Knowledge-Based Systems* 295 (2024) 111779.

- [54] M. Yang, A. Sowmya, An Underwater Color Image Quality Evaluation Metric, *IEEE Transactions on Image Processing* 24 (12) (2015) 6062–6071.
- [55] L. K. Choi, J. You, A. C. Bovik, Referenceless Prediction of Perceptual Fog Density and Perceptual Image Defogging, *IEEE Transactions on Image Processing* 24 (11) (2015) 3888–3901.
- [56] K. Gu, W. Lin, G. Zhai, X. Yang, W. Zhang, C. W. Chen, No-Reference Quality Metric of Contrast-Distorted Images Based on Information Maximization, *IEEE Transactions on Cybernetics* 47 (12) (2016) 4559–4565.
- [57] J. Ke, Q. Wang, Y. Wang, P. Milanfar, F. Yang, MUSIQ: Multi-Scale Image Quality Transformer, in: *Proceedings of the IEEE/CVF International Conference on Computer Vision, IEEE/CVF, Virtual, 2021*, pp. 5148–5157.